International Journal of Microwave and Wireless Technologies

cambridge.org/mrf

A compact automotive antenna module with low coupling between mobile and satellite antennas

Maximilian Holzner, Josua Ephraim Immanuel Buschmann and Stefan Lindenmeier

Institute of High Frequency Technology and Mobile Communication, Universität der Bundeswehr München, Munich, Germany

Research Paper

Cite this article: Holzner M, Buschmann JEI, Lindenmeier S (2026) A compact automotive antenna module with low coupling between mobile and satellite antennas. *International Journal of Microwave and Wireless Technologies*, 1–11. https://doi.org/10.1017/S1759078726103651

Received: 31 December 2025 UTC
Revised: 2 July 2026 UTC
Accepted: 4 July 2026 UTC

Keywords:
5G; automotive; broadband; GNSS; multi-antenna system; multi-band; small mounting area; terrestrial satellite communication; V2X; Wi-Fi

Corresponding author: Maximilian Holzner; Email: m.holzner@unibw.de

Abstract

A new compact automotive multi-antenna module is presented for 5G multiple-input multiple-output applications, as well as Satellite Digital Audio Radio Systems (SDARS) and Global Navigation Satellite System (GNSS) applications in the L1 and L5 bands. The new design consists of two broadband monopole Palm tree antennas for 5G mobile services between 0.6 and 5 GHz, where one of them is surrounded by an SDARS Scarabeus ring antenna, while the other one is surrounded by a novel octagonal dual-band GNSS antenna. This way, every 5G antenna shares its footprint with an antenna for satellite reception. The antennas are combined on a very small area of 114 mm by 56 mm within a height of 26 mm. All of the antennas are designed for low mutual coupling and omnidirectional radiation patterns for the desired elevation angles. In this framework, we introduce a new octagonal GNSS Scarabeus ring antenna, which yields an especially low influence on the matching of the 5G antennas and their antenna patterns. The new antenna concept is verified by way of simulations. A hardware prototype is realized, and antenna measurements are shown, which prove its performance.

Introduction

With the progressing development and expansion of the automotive sector, more and more driving assistance systems are being implemented in vehicles. While, in the beginning, car antennas were mostly used for entertainment purposes, such as music radio broadcasts at low frequencies, nowadays, in addition to entertainment services such as Satellite Digital Audio Radio Systems (SDARS) [1], terrestrial mobile communication services have become common, including 5G multiple-input multiple-output (MIMO), Wi-Fi, and vehicle-to-vehicle (V2V), vehicle-to-infrastructure (V2I), and vehicle-to-everything (V2X) communication [2, 3]. For such high-end applications, the quality of Global Navigation Satellite System (GNSS) signals is also very necessary for precise positioning. The extensive use of many automotive-relevant services and applications leads to a high amount of antenna designs with a lot of diverse antennas within a small mounting area to place them, for example, underneath a shark fin cover [4–9] or in a small module underneath plastic parts of the car's skin. The growing usage of MIMO technology leads to the necessity of more than one terrestrial antenna. To meet the requirements of the state of the art, the monopole antennas occur as a twin constellation. Especially because of safety issues, it is essential to use high-performance antennas to ensure a safe communication connection. The main challenge is to accommodate all antenna elements in a confined space while keeping good performance. In [7], a small-sized antenna set has been introduced with two new wideband Palm tree antennas for 5G mobile services, which are formed in a way that two Scarabeus ring antennas for satellite services could be placed underneath without restrictions on their performance. Nevertheless, the performance of a Palm tree antenna was still partly reduced by resonant modes that occurred in the GNSS Scarabeus antenna.

In this contribution, we introduce a new compact set of 5G, GNSS, and SDARS antennas with a novel type of octagonal Scarabeus satellite antenna and optimized Palm tree antennas, where the Palm tree antennas are no longer influenced by the presence of the satellite antennas and where the satellite antennas keep their good performance. The multi-antenna module consists of two Palm tree antennas for 5G MIMO, Wi-Fi, and V2X, operating in the sub-6 GHz frequency ranges of 617–960 MHz and 1.45–5.925 GHz, as well as satellite antennas for dual-band GNSS in the frequency bands of 1.164–1.214 GHz and 1.559–1.591 GHz and for SDARS from 2.32 to 2.345 GHz, which are compressed together in a small cuboid volume of 114 mm length by 56 mm width by 26 mm height. Simulation and measurement results for the new octagonal

© The Author(s), 2026. Published by Cambridge University Press in association with The European Microwave Association. This is an Open Access article, distributed under the terms of the Creative Commons Attribution licence (http://creativecommons.org/licenses/by/4.0), which permits unrestricted re-use, distribution and reproduction, provided the original article is properly cited.

Downloaded from https://www.cambridge.org/core. UNIVERSIDAD AUTONOMA METROPOLITANA, on 17 Nov 2026 at 16:31:57, subject to the Cambridge Core terms of use, available at https://www.cambridge.org/core/terms. https://doi.org/10.1017/S1759078726103651

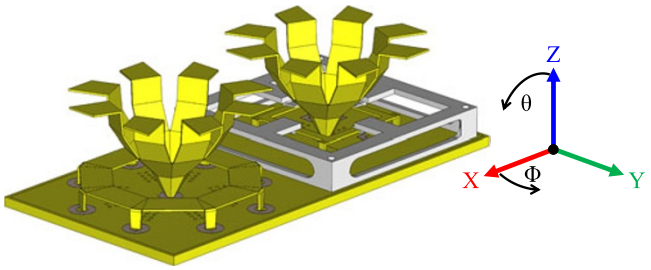


Figure 1. CST model of the compact multi-antenna module.

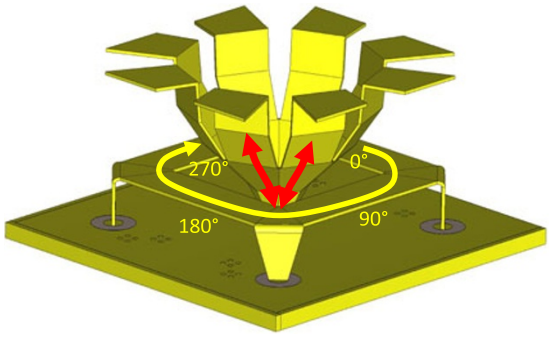


Figure 2. Schematic visualization of orthogonal current distributions between a Palm tree and a Scarabeus antenna.

GNSS antenna show good performance and a strongly increased performance of the Palm tree antenna, which is placed in its center. An earlier version of this paper was presented at the EuMW 2025 Conference and was published in its proceedings [10].

Design and simulation

Design of the antenna module

The following multi-antenna module intends to be able to place all antennas in a small area of 114 mm by 56 mm, with a total height of the highest antenna of 26 mm. For the design of such a compressed module, it is necessary that the large wideband antennas for 5G mobile services can be placed above the flat satellite antennas to share the same small area. So, all antennas are performing in a very low volume with each other. In Figure 1, the complete model of the compact automotive multi-antenna system module is pictured. It shows two Palm tree antennas for 5G, which are placed inside the octagonal GNSS Scarabeus ring antenna (front) and the square SDARS Scarabeus antenna (rear), while most of the typical multi-antenna systems have their terrestrial antenna elements next to their satellite antenna elements [4, 15]. In the literature, there are only a few contributions that show the function of two or more 5G antennas, which cover the frequency range between 617 MHz and 6 GHz and contain the GNSS bands L1 and L5, to compare with. In Table 1, some of them are shown. As it is not easy to compare different systems with different forms of presentation, the table strives to create a fair comparison. As can be seen, the overall size of our proposed antenna module is one of the examples with the smallest volume requirements. There are some more antenna systems, containing terrestrial and satellite antenna combinations [16–20]. As we can see in Figure 1, the distance between each antenna and the others is very small. This makes it necessary to optimize the

Table 1. Automotive antenna modules with wideband terrestrial antennas

Work	PCB size (l × w) and the largest antenna height in mm	Spacing between terrestrial antennas in mm	Highest mutual coupling value appearing between the terrestrial antennas in dB	Highest envelope correlation coefficient value appearing between the terrestrial antennas	Whole frequency-range in GHz without gaps	Applications
[7]	(122 × 60) antenna height: 22	Middle points of the antennas: 60 inner edges: 19.9	<−12	Not given	0.617–5.5	5G, V2X, GNSS L1&L5, SDARS
[9]	(120 × 60) antenna height: 52	19.4	<−9.6	<0.15	0.824–5.925	LTE, GNSS L1, WLAN, Wireless Access in Vehicular Environment (WAVE)
[11]	(180 × 80) antenna height: 49.5	48.5 × 30 × 49.5	−6	<0.4	0.617–6	2 × 2 5G MIMO
[12	Shark-fin housing: (152 × 58) antenna height: 55	12	−6	<0.3	0.698–2.69	LTE, FM, GPS
[13]	(120 × 80) antenna height: 52	Not given	−22.1/−23.8	Not given	0.698–6	LTE, WLAN, V2V, GNSS L1
[14]	Shark-fin housing: (160 × 61.5) antenna height: 50 mm	Not given	<−10	<0.2	1.19–2.8	LTE, WLAN, GNSS BeiDou B1
This work	(114 × 56) antenna height: 26	Middle points of the antennas: 57 inner edges: 12	−10.5	<0.05	0.617–5.925	5G, V2X, GNSS L1&L5, SDARS

Downloaded from https://www.cambridge.org/core. UNIVERSIDAD AUTONOMA METROPOLITANA, on 17 Nov 2026 at 16:31:57, subject to the Cambridge Core terms of use, available at https://www.cambridge.org/core/terms. https://doi.org/10.1017/S1759078726103651

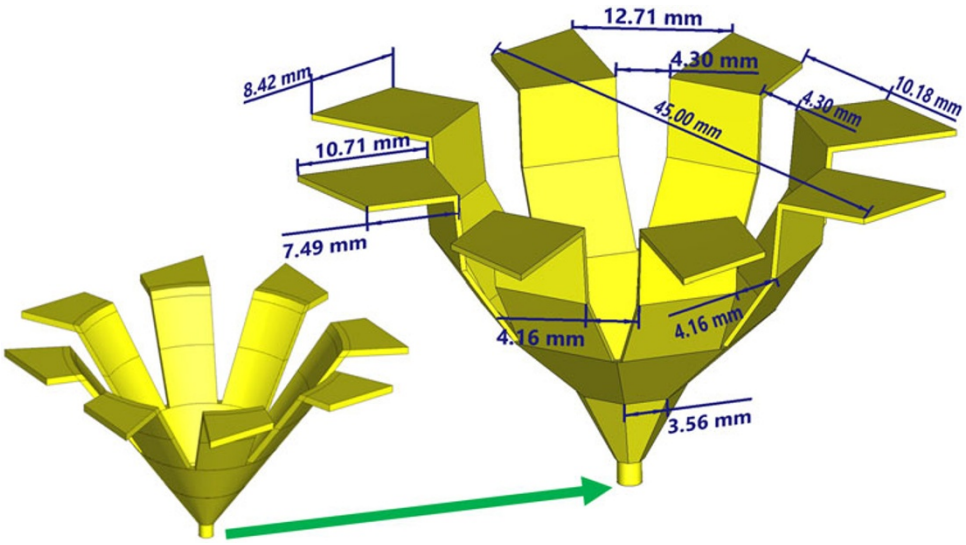


Figure 3. Main evolution steps of the Palm tree antenna.

physical parameters of every single antenna. In the following sections, we focus on the duality of the Palm tree antennas and a novel dual-band GNSS Scarabeus antenna.

Palm tree antenna

One basic antenna type of the multi-antenna system is the broadband-capable linearly polarized Palm tree antenna, which acts in a monopole mode. It combines a conical form for wideband coverage of frequencies from 1.4 to 6 GHz with a roof capacitor for coverage of the low-frequency band from 617 to 960 MHz and is easy to realize. Because of the skin effect, the antenna can be designed hollow in the middle, which reduces weight and material. A special property of the antenna is its vertical slots, which make it possible to place circularly polarized ring-like Scarabeus antennas underneath the Palm tree antenna and around their octagonal cones. These slots are sufficient to minimize the influence of the circularly polarized field on the satellite Scarabeus ring antennas.

The current distributions of the two antennas are predominantly orthogonal, as we can see in Figure 2, which reduces electromagnetic coupling between them. This orthogonality minimizes mutual interaction and preserves the individual radiation characteristics of both antennas despite their close spatial integration, thereby enabling the Palm tree antenna to be positioned at the center of the Scarabeus structure. Since the feeding point of the Palm tree antenna is in the center of the ring antenna and since the currents along the ring antenna (yellow) are rotating around it in phase from 0° to 360°, their overall influences on a vertical current at the feed point (red) of the Palm tree antenna compensate each other.

The appearance of this specially formed monopole antenna leads to the name "Palm tree." As in [7], where a variant of the Palm tree antenna has already been presented, in this contribution, the design develops from a four-level structure to optimize the respective heights in order to minimize mutual coupling effects with other antennas in the proximity of the Palm tree antenna. As it started from a round structure, the cone itself is now designed as an octagonal geometric structure, making it possible to fabricate it from a planar sheet of metal and finally bend it into the final structure and form horizontal elements, which act as a roof capacitor. An evolution of the main Palm tree stages is shown in Figure 3.

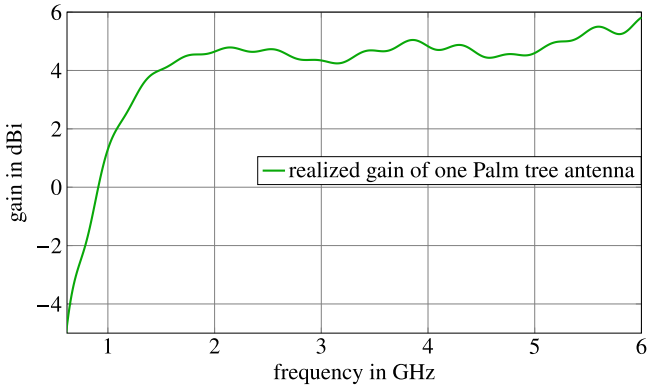


Figure 4. Simulated realized gain over frequency of one Palm tree antenna at $\Phi = 270°$, $\Theta = 90°$.

The gain in the horizontal direction for a single simulated omnidirectionally radiating Palm tree antenna is plotted over frequency in Figure 4.

We recognize a low gain in the 5G low-band from 617 to 960 MHz due to the natural mismatch of such a compact monopole-like antenna. To counter this mismatch, the Palm tree antennas are able to use a multi-stage matching network. The realized gain of the Palm tree antennas in the constellation of Figure 1 is plotted in Figure 5 for the Palm tree antenna in the center of the SDARS Scarabeus antenna, and in Figure 6 for the Palm tree antenna in the center of the GNSS Scarabeus antenna.

In comparison with some other applications of terrestrial antennas in such close proximity, the radiation patterns show a good omnidirectional behavior with a gain of typically around 4 dB in the horizontal plane and dimples of 0 dB gain at frequencies of more than 5 GHz [21].

Downloaded from https://www.cambridge.org/core. UNIVERSIDAD AUTONOMA METROPOLITANA, on 17 Nov 2026 at 16:31:57, subject to the Cambridge Core terms of use, available at https://www.cambridge.org/core/terms. https://doi.org/10.1017/S1759078726103651

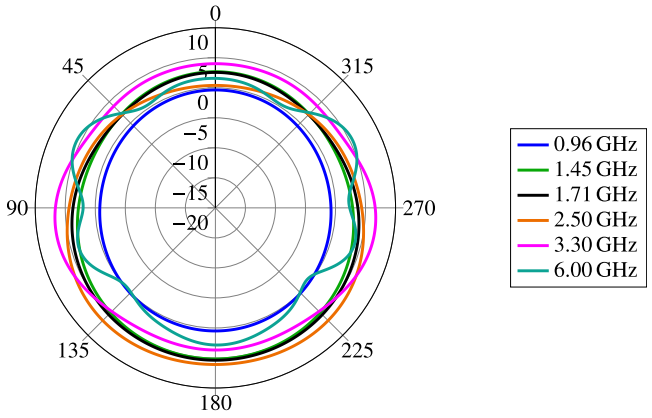


Figure 5. Simulated realized gain of the Palm tree antenna inside the SDARS Scarabeus at a cross section of $\Theta = 90°$ in dBi.

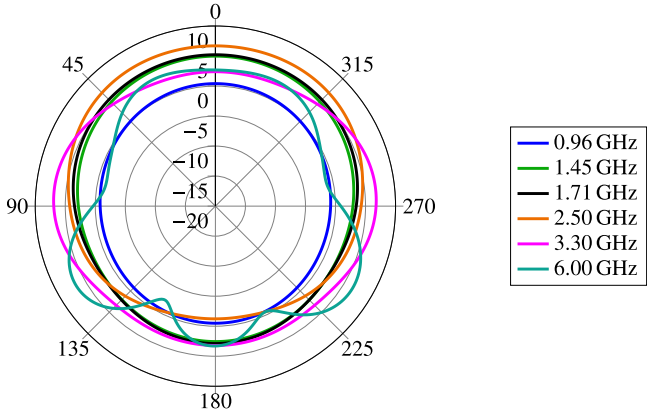


Figure 6. Simulated realized gain of the Palm tree antenna inside the GNSS Scarabeus at a cross section of $\Theta = 90°$ in dBi.

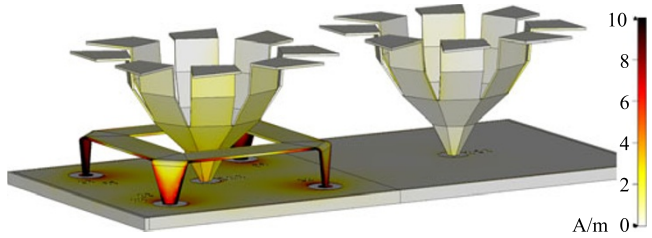


Figure 7. Magnitude of surface current distribution in four-foot Scarabeus scenario when the GNSS-side Palm tree antenna is excited at 3.1 GHz.

Novel GNSS Scarabeus antenna

For GNSS communication purposes, a new Scarabeus-type antenna is deployed. The Scarabeus antenna is a ring antenna with vertical elements in order to shorten the size of the ring. Placed at a distance above the PCB, the Scarabeus antenna performs with low losses as a result of the surrounding air. Through correct design, a Scarabeus antenna is able to cover more L-bands simultaneously [22]. Scarabeus antennas are based on a horizontal ring structure, where, in the resonant radiation mode, one guided wave propagates along the ring structure with one wavelength fitting in. Up to now, four additional vertical elements have been used to shorten the ring while keeping its resonant behavior. The Scarabeus ring structure makes it ideal to be placed underneath a terrestrial antenna of

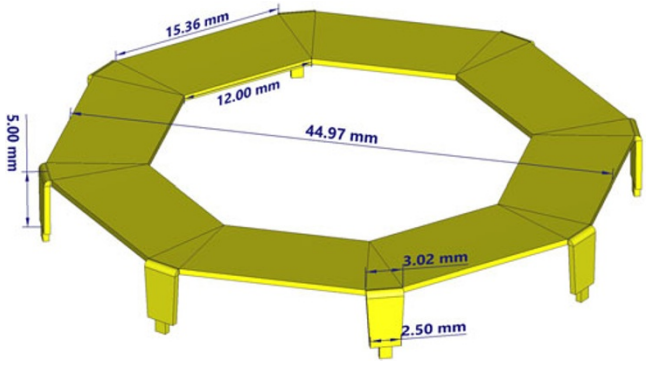


Figure 8. CST model of novel octagonal dual-band Scarabeus antenna.

monopole type. As mentioned before, the Palm tree antenna does not disturb the very good performance of Scarabeus ring antennas, even in the case where this wideband antenna totally covers the Scarabeus ring antenna.

However, the Palm tree antenna itself, which should cover frequencies between 0.6 and 6 GHz, is influenced by resonant modes on the Scarabeus antenna at frequencies close to 3 GHz, where each quarter of the square Scarabeus antenna forms a resonating structure, as can be seen in Figure 9. This behavior can be illustrated very well by the surface current distribution. In Figure 7, we can see the resulting magnitude of the surface current distribution when the left-side Palm tree antenna is excited at 3.1 GHz. The Palm tree antenna induces a surface current at every resonant length of the surrounding four-foot Scarabeus antenna, which also oscillates in monopole mode. Every quarter of the Scarabeus antenna now acts as a parasitic radiator, changing the input impedance of the Palm tree antenna in the center, resulting in a mismatch characteristic.

This is why we now introduce a new octagonal concentric Scarabeus antenna with eight vertical elements, as can be seen in Figure 8. For this structure, the same desired resonant behavior is performed for the GNSS frequencies at L1 and L5 bands. But in contrast to the square Scarabeus antenna, higher-order resonances are suppressed, which would harm the performance of the wideband Palm tree antenna.

So, the idea of the new octagonal Scarabeus antenna is to split the resonant length of the resonant quarters of the square Scarabeus antenna by two, as it is illustrated in Figure 9, and to shift the resonance to higher frequencies above 5 GHz.

In Figure 9, the two Scarabeus antennas are compared. On the left side, the resonant currents of the square Scarabeus quarters in monopole mode are depicted. Their resonant length is close to $\lambda/4$. On the right side of Figure 9, it is visible that the corresponding resonant length of one-eighth of the octagonal Scarabeus is shorter. This way, its resonant frequency is higher. The impact of the resonant length reduction on the surface current distribution can be seen in Figure 10, where we notice an attenuation of the surface current magnitude at the GNSS antenna, while it is high at the Palm tree antenna itself, creating a higher radiation efficiency and total efficiency.

To validate the statement, a direct comparison of the impact of the different Scarabeus types is given in Figure 11. There, the S-parameters of the Palm tree twin antennas are examined when placed in one case inside a four-foot dual-band GNSS antenna, as seen in Figure 7, and in the other case inside the novel eight-foot octagonal dual-band GNSS antenna, as seen in Figure 10. For

Downloaded from https://www.cambridge.org/core. UNIVERSIDAD AUTONOMA METROPOLITANA, on 17 Nov 2026 at 16:31:57, subject to the Cambridge Core terms of use, available at https://www.cambridge.org/core/terms. https://doi.org/10.1017/S1759078726103651

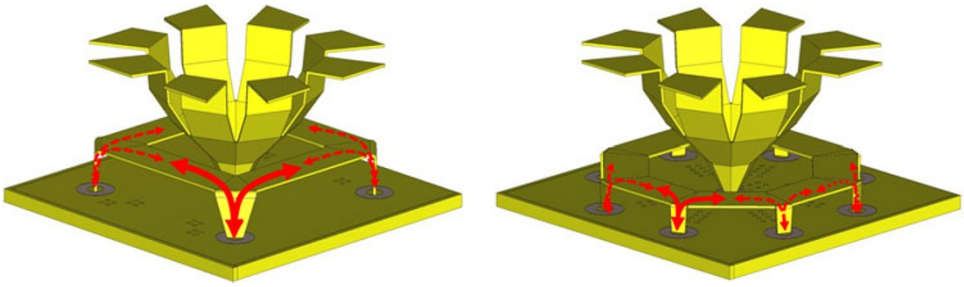


Figure 9. CST models of the four-foot dual-band Scarabeus antenna and novel octagon dual-band Scarabeus antenna with comparison of their respective resonant lengths in monopole mode (red) when attached to a Palm tree antenna.

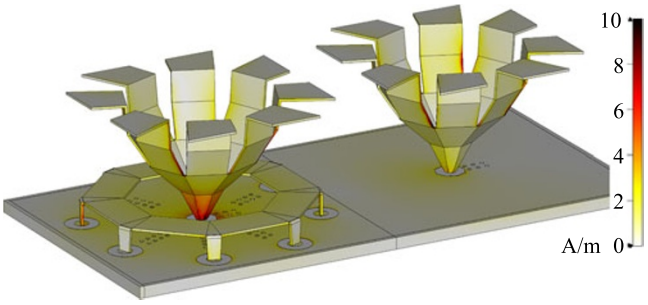


Figure 10. Magnitude of surface current distribution in the novel octagonal Scarabeus scenario when the GNSS-side Palm tree antenna is excited at 3.1 GHz.

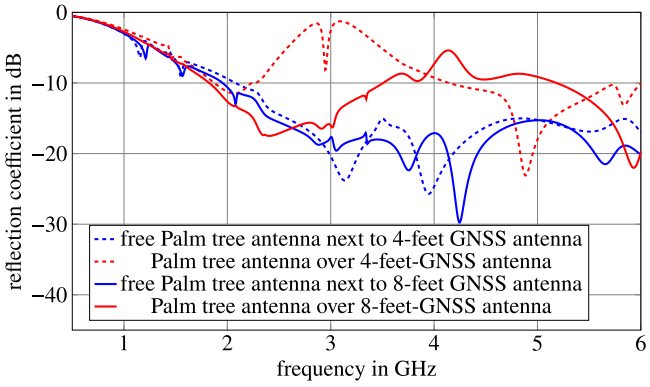


Figure 11. Comparison of Palm tree twin reflection coefficients in different Scarabeus type scenarios. Reflection coefficient shown for the pure radiators, without a matching network.

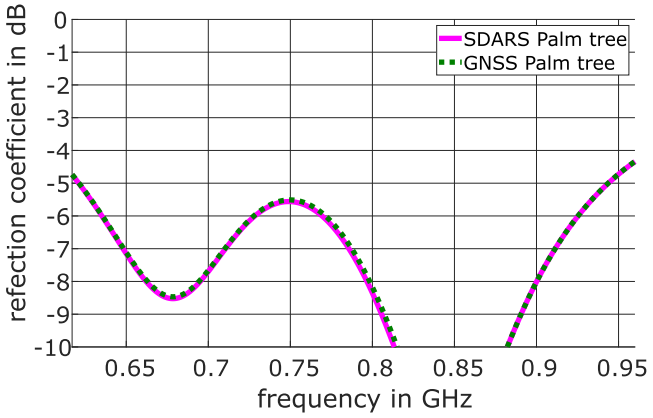


Figure 12. Example of low-band (617–960 MHz) matching of Palm tree antennas in the module.

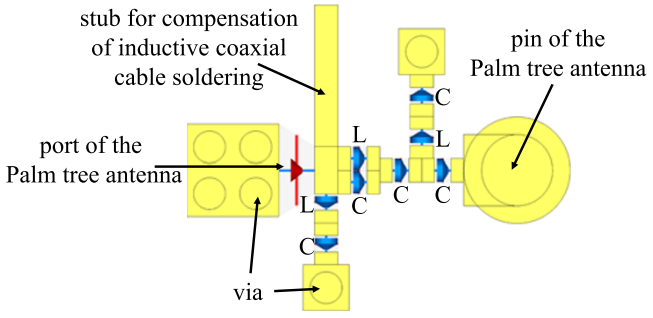


Figure 13. CST layout of low-band (617–960 MHz) multi-stage matching network of the Palm tree antennas in the overall system.

the comparison, the raw S-parameters of the antenna radiators are shown, without a matching network.

As expected, the reduced resonant length leads to an increase in the spurious resonance frequency by 1.3 GHz and an additional suppression of the reflection coefficient by more than 4 dB. An even stronger suppression of the reflection coefficient of the Palm tree antenna inside the GNSS Scarabeus antenna could be achieved by further reducing the coupling-capable resonant length if we use a higher number of vertical elements. The significant improvement qualifies the novel Scarabeus type for deployment under the operating conditions mentioned before.

In order to match the Palm tree antennas also at the low-band between 617 and 960 MHz, a further matching network can be included consisting of a series capacitor, a ground connection via, a series resonant circuit and a capacitor, as well as a parallel resonant circuit in series. Figure 12 shows an example of such matching of two Palm tree antennas in the module together with the octagonal GNSS Scarabeus, where the Palm tree antennas have even a 4 mm lower height, still obtaining matching of typically better than −6 dB. The CST layout of this matching network, applied in the overall system from Figure 1, can be seen in Figure 13.

By inserting this matching network into this contribution, we can observe the resulting reflection coefficient and the resulting realized gain of the Palm tree antennas in Figure 14. An optimization of the circuitry is in progress. We also notice good decoupling, mainly lower than −10 dB.

The simulated envelope correlation coefficient (ECC) is shown in Figure 15, which is determined from the S-parameters of the Palm tree antennas with this multi-stage matching network. ECC

Downloaded from https://www.cambridge.org/core. UNIVERSIDAD AUTONOMA METROPOLITANA, on 17 Nov 2026 at 16:31:57, subject to the Cambridge Core terms of use, available at https://www.cambridge.org/core/terms. https://doi.org/10.1017/S1759078726103651

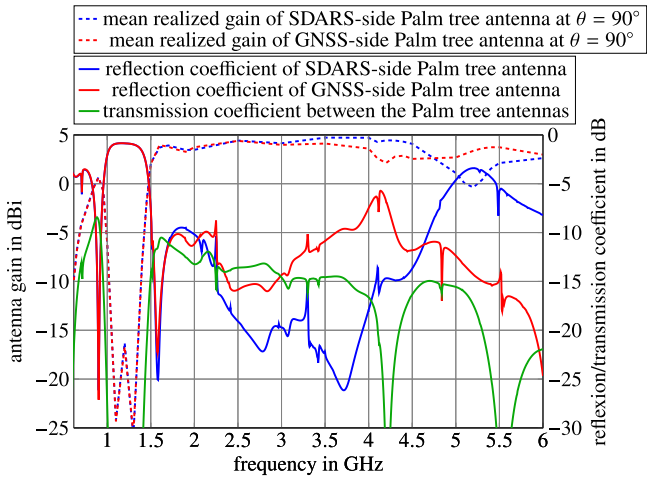


Figure 14. Reflection coefficient, coupling, and resulting realized gain of the Palm tree antennas with a multi-stage matching network.

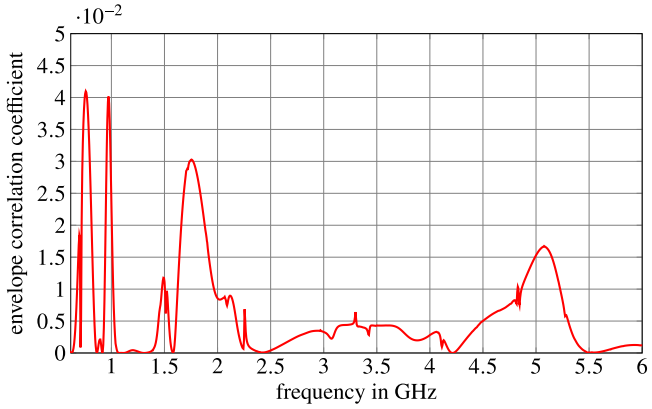


Figure 15. Simulated ECC from the S-parameters of the Palm tree antennas with a multi-stage matching network.

is a performance criterion for cross-correlation behavior and channel capacity [9, 14, 23], where values lower than 0.5 at the mobile side are considered to be suitable for MIMO applications. As can be seen in Figure 15, the highest value of ECC is below 0.045 in the considered multi-antenna system, which is caused by its low transmission parameters and a helpful phase difference between reflection and transmission parameters. With that, the multi-antenna system is practicable for MIMO deployment.

Now we consider the performance of the new octagonal GNSS Scarabeus antenna, which is simulated together with the complete antenna module. With just a most unpretentious matching network consisting of series capacitors, recognizable in Figure 16, where the bottom side of the PCB at the GNSS side is pictured, a dual-band matching is realized also for the Scarabeus antenna.

Figure 17 plots the simulated reflection coefficient of the novel dual-band GNSS Scarabeus antenna implemented in the overall system, shown in Figure 1. Figure 18 shows the simulated IEEE gain of the octagonal GNSS Scarabeus antenna when inserted in the overall system at 1.2 GHz. Figure 19 shows the same situation for 1.575 GHz. The performance in the overall system is described with the cross-polarization discrimination (XPD) between right-hand circularly polarized gain and left-hand circularly polarized gain. As we can see, an excellent XPD of more than 20 dB and an

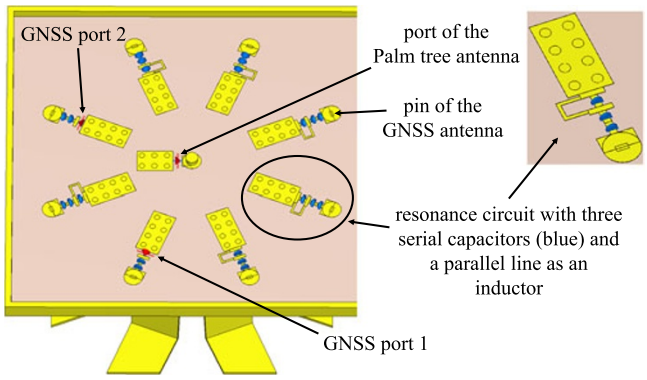


Figure 16. GNSS backside of the PCB with respective circuits and feeds.

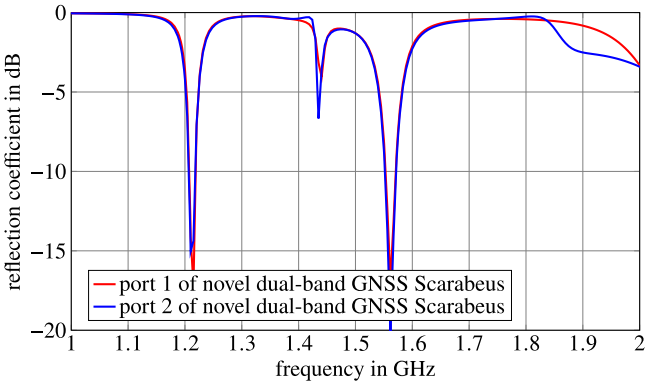


Figure 17. Simulated reflection coefficient of the novel dual-band GNSS Scarabeus at its two ports.

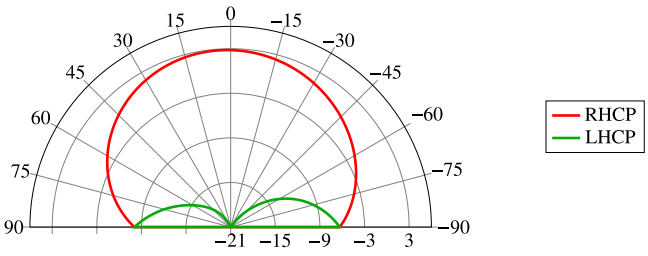


Figure 18. Simulated IEEE gain of the novel octagon GNSS Scarabeus at 1.2 GHz and Phi = 0° in dBi.

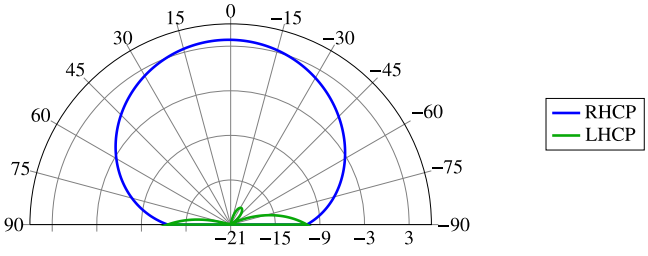


Figure 19. Simulated IEEE gain of the novel octagon GNSS Scarabeus at 1.575 GHz and Phi = 0° in dBi.

axial ratio (AR) close to 1 are achieved even in the presence of the Palm tree antenna. The good XPD is also obtained at the other frequency samples of the proposed frequency bands, as we can see in

Downloaded from https://www.cambridge.org/core. UNIVERSIDAD AUTONOMA METROPOLITANA, on 17 Nov 2026 at 16:31:57, subject to the Cambridge Core terms of use, available at https://www.cambridge.org/core/terms. https://doi.org/10.1017/S1759078726103651

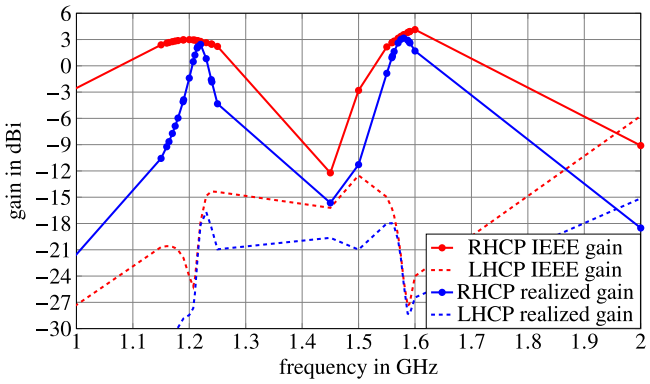


Figure 20. Simulated gain over frequency of the novel dual-band GNSS Scarabeus antenna.

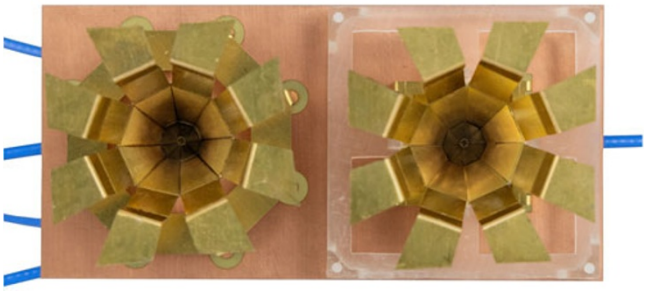


Figure 21. Prototype model of compact multi-antenna module from top view.

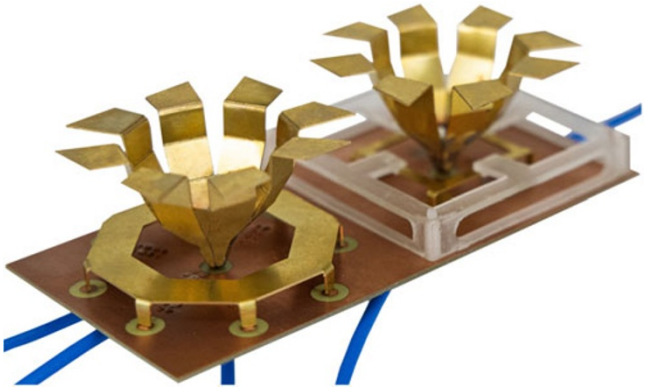


Figure 22. Prototype model of compact multi-antenna module.

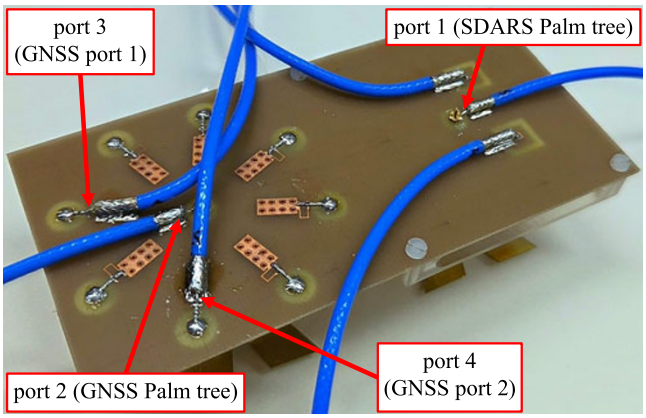


Figure 23. Prototype model of compact multi-antenna module from bottom view with respective ports.

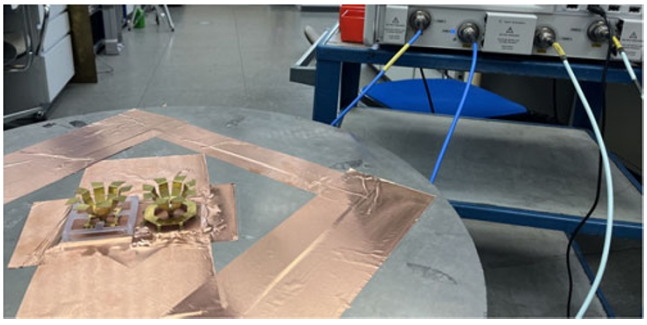


Figure 24. S-parameter measurement setup.

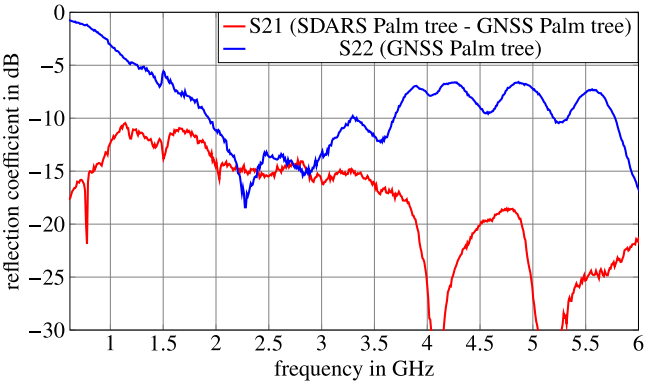


Figure 25. Measured S-parameters of Palm tree antennas without a matching network.

Figure 20, where the IEEE gain and the realized gain of the novel octagonal dual-band Scarabeus antenna are plotted over frequency.

We notice a broadband XPD behavior at the L1, L2, and L5 GPS bands with a respective high IEEE gain for the right-hand polarization. For this contribution, we decided to use an easy dual-band-capable network because this is sufficient to prove the obtained performance of the novel octagon GNSS Scarabeus antenna while covered by a Palm tree antenna in its center. The radiation efficiency of the dual-band octagon GNSS is in the region of −3 and −4 dB, which is caused by the dual-band resonant network. For single-frequency applications, we get values in the region of −1.5 and −2 dB. In the actual state of the design, there is still potential left to improve the efficiency significantly. More than 20% of the losses are caused by the loss tangent of the cheap FR-4 substrate. Around 10% of the losses are caused by the circuitry, which can be further improved in its design. Also, the metal plating can be changed, which actually leads to 30% of the losses. This way, we can estimate a further increase of 1–2 dB in efficiency for further design iterations.

Realization

A hardware model is realized in the laboratories and the workshop of our institute of high frequency technology at the University of the Bundeswehr in Munich to serve as a first prototype in order to prove its antenna performance. The new antenna module can be seen in Figures. 21–23 in different perspectives.

Downloaded from https://www.cambridge.org/core. UNIVERSIDAD AUTONOMA METROPOLITANA, on 17 Nov 2026 at 16:31:57, subject to the Cambridge Core terms of use, available at https://www.cambridge.org/core/terms. https://doi.org/10.1017/S1759078726103651

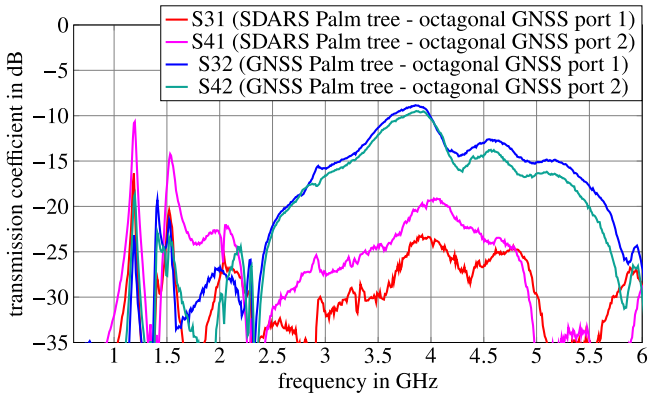


Figure 26. Measured transmission coefficients between the Palm tree antennas and the octagonal GNSS Scarabeus.

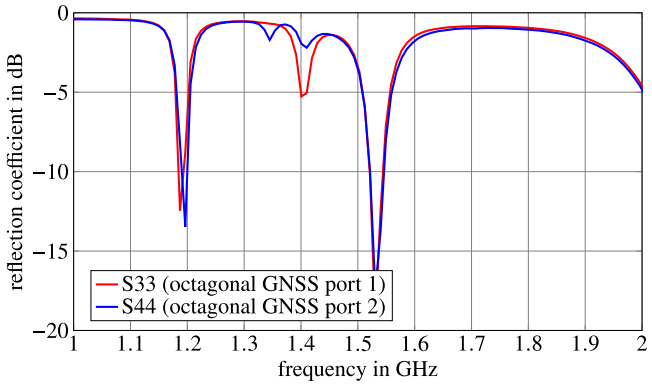


Figure 27. Measured reflection coefficient of the novel octagonal dual-band GNSS Scarabeus.

The PCB is laser-processed from a piece of FR-4 substrate, which creates the base of the compact multi-antenna system module. As FR-4 is an industrial standard antenna PCB because of its reliability and cost efficiency for mass production, it is the substrate of choice for this multi-antenna system [24, 25]. With a relative permittivity of nearly 4.3 and a loss tangent of nearly 0.025, it provides more losses, especially for the octagonal dual-band GNSS Scarabeus. A change to a lower-loss substrate compared to FR-4 could minimize the losses and maximize the efficiencies, but makes the antenna system more expensive. Nevertheless, in this contribution, it is shown that the antennas, especially the GNSS antenna, achieve a realized gain near 3 dBi. Holes are drilled for the Palm tree antennas, GNSS Scarabeus, SDARS holder, and via connections. All antenna elements are milled out of 0.5 mm sheets of brass and bent to the intended 3D structure. As can be seen in Figure 21, the 5G Palm tree antennas completely cover the antennas for satellite reception.

Measurements

In the following, measurements of the first prototype of the compact antenna module are shown. The measurements have been performed in the laboratories and the anechoic chamber of the Institute of High Frequency Technology.

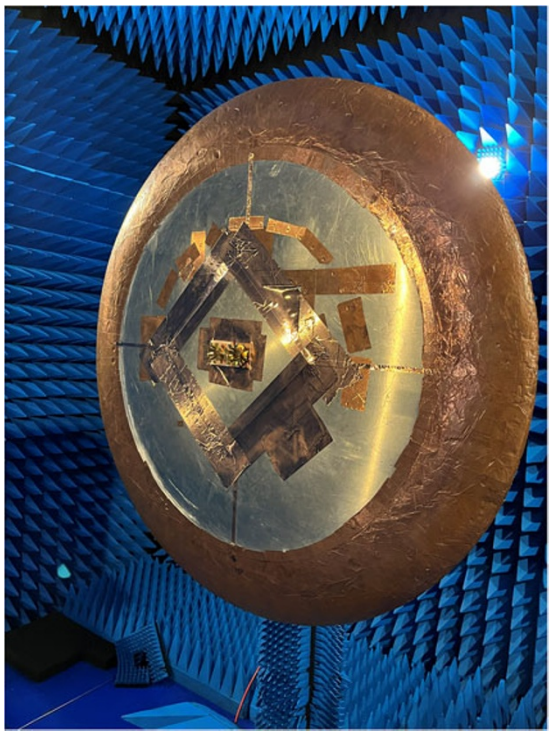


Figure 28. Far-field measurement setup in the anechoic chamber.

Measurement of scattering parameters

The scattering parameters of the compact multi-antenna module are measured with a Vector Network Analyzer on an extended ground plane. In Figure 24, we can see the setup for the S-parameter measurement.

As mentioned before, one of the main challenges of multi-antenna systems in a small accommodation area is the coupling between the respective antennas. Therefore, we have to pay particular attention to the coupling parameters. In Figure 25, we can see the measured transmission coefficient between the linearly polarized terrestrial Palm tree antennas as well as the measured reflection coefficient of the GNSS-side Palm tree antenna.

Because of the extremely compact module and an antenna distance of only 57 mm, the mutual coupling in this structure is relatively high. But as can be shown by simulation results in Figure 14, the coupling can still be kept mainly lower than −10 dB even with a matching circuit because of its additional losses. For further discussion, we concentrate on frequencies above 1 GHz, due to the usual mismatch of the Palm tree antennas in the 5G low-band, caused by the small height of the antennas. In Figure 25, we can see a coupling of −10 dB at maximum for frequencies up to 2 GHz. For higher frequencies, a coupling of around −15 dB is achieved. For frequencies above 3.9 GHz, transmission coefficients of less than −20 dB are measured. For consideration of the coupling between the new octagonal GNSS Scarabeus antenna and the Palm tree antennas, we look at Figure 26, where we recognize two small band maxima peaks in coupling between the SDARS Palm tree and the octagonal GNSS Scarabeus at 1.196 GHz of −10.7 dB and at 1.53 GHz of −14.2 dB. This is not critical since the 5G antennas are not active at these frequencies.

For the rest of the frequencies, the antennas are coupled with typically much less than −20 dB. Looking at the coupling between

Downloaded from https://www.cambridge.org/core. UNIVERSIDAD AUTONOMA METROPOLITANA, on 17 Nov 2026 at 16:31:57, subject to the Cambridge Core terms of use, available at https://www.cambridge.org/core/terms. https://doi.org/10.1017/S1759078726103651

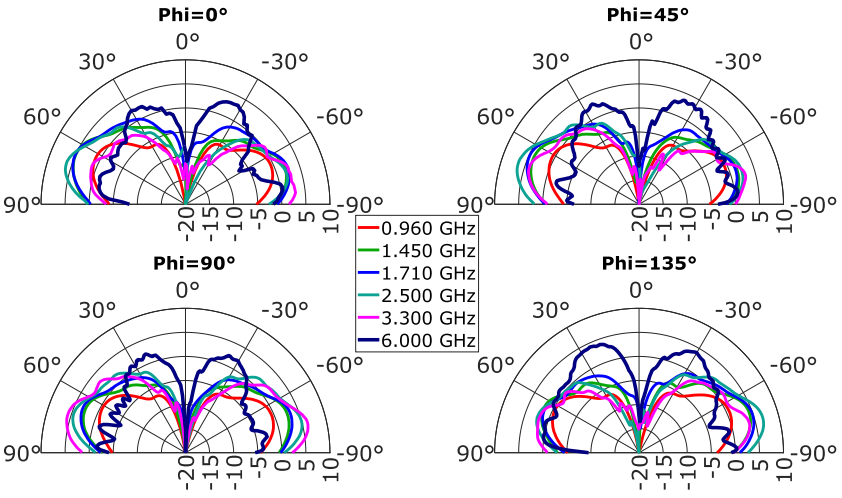


Figure 29. Measured gain of the Palm tree antenna inside the octagonal dual-band GNSS Scarabeus at different vertical cut sections in dBi.

the Palm tree antenna inside the GNSS Scarabeus and the octagonal GNSS Scarabeus, we recognize a peak around 4 GHz with a maximum coupling of slightly more than −10 dB, while at the other frequencies, the antennas are coupled with much lower transmission coefficients. The measurement of the coupling is consistent with the simulated matching of the Palm tree antenna, as shown in Figure 11, where we notice the increase in the reflection coefficient close to 4 GHz.

The big advantage of the octagonal GNSS Scarabeus, next to the reduced coupling compared to a four-foot Scarabeus, is its dual-band capability. Therefore, for this antenna, we have to look at the reflection coefficient in Figure 27, where we recognize two peaks with matching character.

Compared to the simulated reflection coefficient, illustrated in Figure 17, we see good agreement between the graphs. Some slight frequency deviations of the matched peaks are recognizable, which partly originate from fabrication tolerances of the antennas and elements, as well as parasitic effects of the matching circuits, which consist of resonant circuits, realized in SMD technology. Optimization of the system is in progress.

Measurement of far-field antenna patterns

The far-field measurements are performed in the institute's anechoic chamber on a finite ground plane with bent edges and a diameter of 1.2 and 4 m of antenna distance. In Figure 28, the measurement setup for the far-field antenna patterns is shown.

To validate the Palm tree antennas, vertical, horizontal, and half-sphere measurements are performed. Because of the limited ground plane of the measurement setup, the maximum amplitude of the Palm tree antennas is not located at $\Theta = 90°$. Therefore, we look at the vertical plots of the Palm tree antenna inside the octagonal GNSS antenna in Figure 29.

In Figure 29, we notice a very symmetrical structure of the vertical far-field pattern of the respective frequencies for the four azimuthal cut sections. The roundness is emphasized again in Figure 30, where the horizontal pattern of the Palm tree antenna inside the octagonal GNSS antenna is plotted at an elevation angle of $\Theta = 70°$. As we can notice from the simulated results, the measurement results show an overall good roundness of the radiation pattern with low variance in gain for the respective frequencies. In the direction of the other Palm tree antenna, the gain is slightly decreased by 2 dB, while it is increased by 2 dB in the opposite

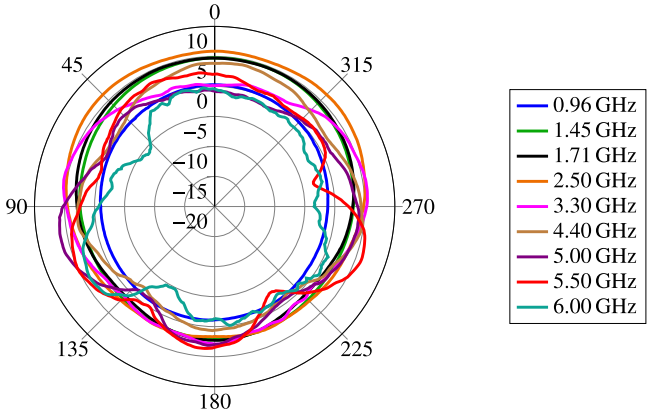


Figure 30. Measured gain of the Palm tree antenna inside the octagonal dual-band GNSS Scarabeus at $\Theta = 70°$ in dBi.

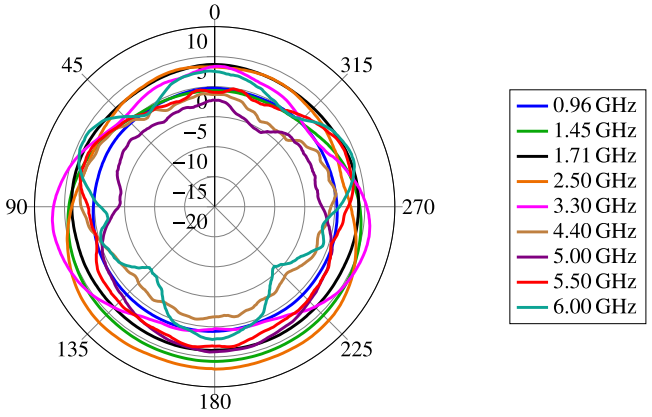


Figure 31. Measured gain of the Palm tree antenna inside the SDARS Scarabeus at $\Theta = 70°$ in dBi.

direction. At higher frequencies, the variances increase, but are still low with respect to the environment of three other antennas.

We also get a similarly advantageous radiation pattern with low variance when we look at the Palm tree antenna inside the SDARS Scarabeus. Figure 31 shows the gain of the SDARS side Palm tree antenna, identical in construction, for the same horizontal cut section at $\Theta = 70°$. Here, there is again an increased gain by 2 dB in

Downloaded from https://www.cambridge.org/core. UNIVERSIDAD AUTONOMA METROPOLITANA, on 17 Nov 2026 at 16:31:57, subject to the Cambridge Core terms of use, available at https://www.cambridge.org/core/terms. https://doi.org/10.1017/S1759078726103651

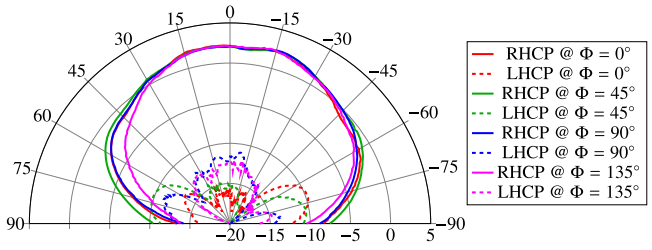


Figure 32. Measured IEEE gain of the octagonal dual-band GNSS Scarabeus antenna at 1.2 GHz in dBi.

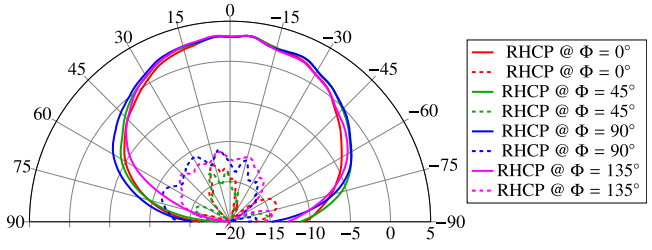


Figure 33. Measured IEEE gain of the octagonal dual-band GNSS Scarabeus antenna at 1.58 GHz in dBi.

the opposite direction of the other Palm tree antenna. This way, the slight variances in gain of the two Palm tree antennas complement each other. In summary, the measurements of the Palm tree antennas show good omnidirectional behavior from the point of view of a compact multi-antenna system of this size. It also proves the functionality in combination with the Scarabeus satellite antenna concept. The next measurements concentrate on the novel octagonal dual-band GNSS Scarabeus antenna. The slight frequency shift in good matching of the reflection coefficient, seen in Figure 27, leads to a slight mismatch at the antenna resonance frequencies. Therefore, to show the potential performance of the dual-band Scarabeus antenna, the IEEE gain is plotted. In Figure 32, the IEEE gain of the octagonal dual-band GNSS Scarabeus antenna is plotted for 1.2 GHz, and in Figure 33 for 1.58 GHz.

For both frequencies, we achieve a measured IEEE gain of around 3 dB, while obtaining an XPD of more than 14 dB at 1.2 GHz and 15 dB at 1.58 GHz. The measurements of the novel octagonal dual-band GNSS Scarabeus antenna show very good agreement with the simulated results. Also, the functionality of this antenna concept in combination with a broadband Palm tree antenna is validated.

Conclusion

A new compact multi-antenna system module consisting of two broadband Palm tree antennas, a dual-band GNSS Scarabeus antenna, and an SDARS Scarabeus antenna is introduced. All antennas are optimized to perform in the presence of the other antennas. For this purpose, a novel kind of circularly polarized octagonal GNSS Scarabeus antenna is presented. The new GNSS antenna shows very good results regarding the gain, the shape of the radiation pattern, and the AR, although it is completely covered underneath the Palm tree antennas. In the presence of the Scarabeus antennas, the Palm tree antennas also show very good wideband performance with a gain of typically 4 dBi in the horizontal direction with omnidirectional behavior in azimuth. Matching in the 5G high bands is especially enabled due to the novel octagonal dual-band GNSS Scarabeus antenna, which leads to low coupling of resonant modes with the Palm tree antennas. An additional 5G low-band matching network is applied, matching the Palm tree antennas in a frequency range between 617 and 960 MHz. The antenna module has been realized as a hardware prototype, and its performance is validated via measurements of scattering parameters and far-field radiation patterns. The measurement results verify the functionality of the Palm tree antennas for 5G and the circularly polarized Scarabeus satellite antennas, while sharing the same footprint. The small footprint area of only 114 mm by 56 mm by 26 mm makes the multi-antenna system ideal for deployment in vehicular applications.

Competing interests. The authors hereby declare that there are no conflicts of interest.

References

1. **Bilgic MM and Yegin K** (2016) Modified annular ring antenna for GPS and SDARS automotive applications. *IEEE Antennas and Wireless Propagation Letters* **15**, 1442–1445. https://doi.org/10.1109/LAWP.2015.2512558
2. **Nguyen AQ, Tran HA, Tran TH and Dao NP** (2021) Implementation of a WiFi-based V2V-V2I communication unit for low speed vehicles. In *International Conference on Advanced Technologies for Communications (ATC)*. Ho Chi Minh City, Vietnam, pp. 79–82. https://doi.org/10.1109/ATC52653.2021.9598224
3. **Corradi RF, Lenzini S, Melli F, Notari A and Vincetti L** (2021) 3D automotive antenna for 5G and V2X communications. In *XXXIVth General Assembly and Scientific Symposium of the International Union of Radio Science (URSI GASS)*. Rome, Italy, pp. 1–4. https://doi.org/10.23919/URSIGASS51995.2021.9560634
4. **Attaran A, Larashi E, Mäurer C and Reddy CJ** (2024) Design and integration of V2X and SDARS antennas in automotive rooftop shark-fin antenna module. In *IEEE International Symposium on Antennas and Propagation and INC/USNC-URSI Radio Science Meeting (AP-S/INC-USNC-URSI)*. Firenze, Italy, pp. 761–762. https://doi.org/10.1109/AP-S/INC-USNC-URSI52054.2024.10686163
5. **Sarwar SM, Chowdhury MFF and Das HS** (2019) A dual band shark fin integrated vehicle antenna for 5G and Wi-Max applications. In *IEEE International Conference on Telecommunications and Photonics (ICTP)*. Dhaka, Bangladesh, pp. 1–4. https://doi.org/10.1109/ICTP48844.2019.9041812
6. **Hasturkoğlu S and Lindenmeier S** (2018) Antenna module with new wideband 5G-antenna array at 28 GHz in combination with GNSS- and 4G/WLAN/DSRC in automotive environment. In *48th European Microwave Conference (EuMC)*. Madrid, Spain, pp. 1073–1076. https://doi.org/10.23919/EuMC.2018.8541591
7. **Panholzer E and Lindenmeier S** (2023) A novel automotive palmtree antenna for 5G inside scarabeus ring antennas for satellite reception. In *53rd European Microwave Conference (EuMC)*. Berlin, Germany, pp. 967–970. https://doi.org/10.23919/EuMC58039.2023.10290700
8. **Toprak Z, Senega S and Lindenmeier S** (2021) A novel automotive ultra-wideband 5G-MIMO-antenna array printed on a foil. In *50th European Microwave Conference (EuMC)*. Utrecht, Netherlands, pp. 216–219. https://doi.org/10.23919/EuMC48046.2021.9338079
9. **Kwon O-Y, Song R and Kim B-S** (2018) A fully integrated shark-fin antenna for MIMO-LTE, GPS, WLAN, and WAVE applications. *IEEE Antennas and Wireless Propagation Letters* **17**(4), 600–603. https://doi.org/10.1109/LAWP.2018.2805681
10. **Holzner M, Buschmann JEI and Lindenmeier S** (2025) A compact automotive multi antenna module with new octagonal GNSS scarabaeus antenna. In *55th European Microwave Conference (EuMC)*. Utrecht, Netherlands, pp. 375–378. https://doi.org/10.23919/EuMC65286.2025.11235260.
11. **Zhou Y, Jiang T, Li H and Chen F** (2024) A 5G MIMO multiband low-profile antenna design for automotive shark-fin systems. *IEEE Antennas*

Downloaded from https://www.cambridge.org/core. UNIVERSIDAD AUTONOMA METROPOLITANA, on 17 Nov 2026 at 16:31:57, subject to the Cambridge Core terms of use, available at https://www.cambridge.org/core/terms. https://doi.org/10.1017/S1759078726103651

and Wireless Propagation Letters **23**(5), 1588–1592. https://doi.org/10.1109/LAWP.2024.3363221
12. **Liu Y, Ai Z, Liu G and Jia Y** (2019) An integrated shark-fin antenna for MIMO-LTE, FM, and GPS applications. *IEEE Antennas and Wireless Propagation Letters* **18**(8), 1666–1670. https://doi.org/10.1109/LAWP.2019.2927019
13. **Wu Q, Zhou Y and Guo S** (2018) An L-sleeve L-monopole antenna fitting a shark-fin module for vehicular LTE, WLAN, and car-to-car communications. *IEEE Transactions on Vehicular Technology* **67**(8), 7170–7180. https://doi.org/10.1109/TVT.2018.2828433
14. **Shen L, Luo W, Miao Y and Liu G** (2024) Combined shark-fin rooftop antenna for LTE, WLAN and BeiDou applications. *Electronics* **13**, 1324. https://doi.org/10.3390/electronics13071324
15. **Yacoub A and Aloi DN** (2022) Low-Profile Automotive Antenna Systems for MIMO 5G and L1/L5 GNSS Communications. In *16th European Conference on Antennas and Propagation (EuCAP)*. Madrid, Spain, pp. 1–4. https://doi.org/10.23919/EuCAP53622.2022.9769623
16. **Nikam AA and Patil RB** (2023) Integration of LTE and GNSS antenna for multiband performance in vehicular application. *Progress In Electromagnetics Research C* **134**, 157–169. https://doi.org/10.2528/PIERC23051603
17. **Salah AZ and Eibert TF**, (2025) Compact, highly decoupled antennas for automotive SDARS, WiFi, and V2X applications. In *19th European Conference on Antennas and Propagation (EuCAP)*. Stockholm, Sweden, pp. 1–3. https://doi.org/10.23919/EuCAP63536.2025.10999219
18. **Skanda S, Satish S, Kodaganur AN and Shanthi P** (2023) Design of shark-fin superstrate antenna for 5G and GPS applications. In *7th International Conference on Computation System and Information Technology for Sustainable Solutions (CSITSS)*. Bangalore, India, pp. 1–5. https://doi.org/10.1109/CSITSS60515.2023.10334230
19. **Ghafari E, Fuchs A, Eblenkamp D and Aloi DN** (2014) A vehicular rooftop, shark-fin, multiband antenna for the GPS/LTE/cellular/DSRC systems. In *IEEE-APS Topical Conference on Antennas and Propagation in Wireless Communications (APWC)*. Aruba: Palm Beach, pp. 237–240. https://doi.org/10.1109/APWC.2014.6905546
20. **Goncharova I and Lindenmeier S** (2015) A high efficient automotive roof-antenna concept for LTE, DAB-L, GNSS and SDARS with low mutual coupling. In *9th European Conference on Antennas and Propagation (EuCAP)*. Lisbon, Portugal, pp. 1–5.
21. **Demien C and Sarkis R** (2019) Design of shark fin integrated antenna systems for automotive applications. In *PhotonIcs & Electromagnetics Research Symposium - Spring (PIERS-Spring)*. Rome, Italy, pp. 620–627. https://doi.org/10.1109/PIERS-Spring46901.2019.9017479
22. **Meredov A and Lindenmeier S** (2023) A compact RHCP and LHCP antenna array for L1 and L5 band on a Satellite. In *17th European Conference on Antennas and Propagation (EuCAP)*. Florence, Italy, pp. 1–5. https://doi.org/10.23919/EuCAP57121.2023.10133094
23. **Vaughan RG and Andersen JB** (1987) Antenna diversity in mobile communications. *IEEE Transactions on Vehicular Technology* **36**(4), 149–172. https://doi.org/10.1109/T-VT.1987.24115
24. **Qureshi AA, Afzal MU, Tauqeer T and Tarar MA** (2011) "Performance analysis of FR-4 substrate for high frequency microstrip antennas". In China-Japan Joint Microwave Conference. Hangzhou, China, pp. 1–4.
25. **Tung W-S, Rao P-Z and Chen W-M** (2019) A millimeter-wave antenna on low cost FR4 Substrate. In *IEEE Asia-Pacific Microwave Conference (APMC)*, Singapore, pp. 652–654. https://doi.org/10.1109/APMC46564.2019.9038532



Maximilian Holzner received the B.Sc. and M.Sc. degrees in electrical engineering from the University of the Bundeswehr Munich in 2019 and 2020, respectively. In 2023, he joined the Department for High Frequency Technology as a research assistant and Ph.D. candidate. His research topics focus on satellite and terrestrial antennas for space and automotive applications.



Josua Ephraim Immanuel Buschmann received the B.Sc. degree in electrical engineering from the University of the Bundeswehr Munich in 2025. He is currently pursuing a master's degree in electrical engineering. His research topics focus on combinations of terrestrial and satellite antennas for automotive applications.



Stefan Lindenmeier studied electrical engineering at the Technical University of Munich and joined the Ferdinand Braun Institut fuer Hoechstfrequenztechnik from 1994 to 1996. He obtained the Ph.D. degree in 1996 and the Venia Legendi in High Frequency Technology in 2000, both at the Technical University of Munich, where he was an assistant professor from 1996 to 2000. In 2000, he joined the DaimlerChrysler Research and Technology Centre in Ulm, Germany, where he became leader of the research group for antennas and RF sensors. Since 2004, he has been a full professor and leader of the Department of High Frequency Technology and Mobile Communications at the University of the Bundeswehr in Munich, where he was also dean and member of the senate. He was the IEEE chapter coordinator for Region 8, MTT, AP, and BT, curator of Fraunhofer FHR, and is a member of expert committees in URSI, ITG, and others. His main research topics are antenna technology and reception systems for automotive and satellite applications, as well as electromagnetic field modeling. He is the author of more than 240 scientific publications in these fields of research.

Downloaded from https://www.cambridge.org/core. UNIVERSIDAD AUTONOMA METROPOLITANA, on 17 Nov 2026 at 16:31:57, subject to the Cambridge Core terms of use, available at https://www.cambridge.org/core/terms. https://doi.org/10.1017/S1759078726103651